PCCP

PAPER

View Article Online
View Journal | View Issue

Cite this: *Phys. Chem. Chem. Phys.*, 2018, **20**, 4840

Adsorption and decomposition of dimethyl methylphosphonate on size-selected $(MoO_3)_3$ clusters†

Xin Tang,[a] Zachary Hicks,[a] Linjie Wang,[a] Gerd Ganteför,[b] Kit H. Bowen,*[a] Roman Tsyshevsky,[c] Jianwei Sun[d] and Maija M. Kuklja[c]

Received 16th December 2017,
Accepted 23rd January 2018

DOI: 10.1039/c7cp08427g

rsc.li/pccp

The adsorption and decomposition of dimethyl methylphosphonate (DMMP), a chemical warfare agent (CWA) simulant, on size-selected molybdenum oxide trimer clusters, *i.e.* $(MoO_3)_3$, was studied both experimentally and theoretically. X-ray photoelectron spectroscopy (XPS), temperature programmed reaction (TPR), and density functional theory (DFT)-based simulations were utilized in this study. The XPS and TPR results showed both, desorption of intact DMMP, and decomposition of DMMP through the elimination of methanol at elevated temperatures on $(MoO_3)_3$ clusters. Theoretical investigation of DMMP on $(MoO_3)_3$ clusters suggested that, in addition to pure $(MoO_3)_3$ clusters, reduced molybdenum oxide clusters and hydroxylated molybdenum oxide clusters also play an important role in decomposing DMMP *via* a "reverse Mars–van Krevelen mechanism". The present study, which focused on oxide clusters, underlines the importance of surface defects, *e.g.*, the oxygen vacancies and surface hydroxyls, in determining the reaction pathway of DMMP, in agreement with previous studies on thin films. In addition, the structural fluxionality and the Lewis acidity of molybdenum oxide clusters, *i.e.* $(MoO_3)_3$, may make them good candidates for adsorption and decomposition of chemical warfare agents with similar structures to DMMP.

1 Introduction

Protection from chemical warfare agents (CWAs) requires the development of functional materials and catalysts to remove and/or decompose CWAs in an efficient manner. Regardless of the CWA, its concentration, and method of deployment, a mask or chemical-defense kit remains the best individual protection against chemical agents with the mask being used to protect the face, eyes, and respiratory tract against the hazardous chemical agents. The key component of the mask is the filter material, which is responsible for adsorption and degradation of the chemical agents. Unfortunately, despite its importance to the design of new materials and the improvement of current protective equipment, a detailed understanding of the processes, occurring both on and within the filter material during CWA exposure, is still lacking on the molecular level.

Gas masks have traditionally consisted of carbon-based and metal/metal-oxide-based filter materials and while a range of carbon-based filter material structures and compositions have been heavily studied,[1] most of the experimental studies of the adsorption and decomposition of CWAs and their simulant compounds on metal oxides have been performed on single crystals, polycrystalline films and nanoparticles.[2–15] In many of these experiments it was shown that the mechanisms of adsorption and decomposition depend strongly on the surface structure of the filter material and the presence of contaminants.

Sub-nano clusters, chemical species consisting of a relatively small number of atoms, have been widely studied in the field of heterogeneous catalysis both as catalysts and as model systems used to help explain catalytic processes. Despite their intriguing size-dependent catalytic properties, which are attractive for creating new efficient filter materials, and their uses as model systems, which can help explain reactions at a molecular level, attempts to explore the ability of well-defined clusters to adsorb and degrade CWAs have not been reported.

In this research, we explore the adsorption and decomposition of dimethyl methylphosphonate (DMMP), a CWA simulant, on size-selected $(MoO_3)_3$ trimer clusters deposited on a highly-ordered pyrolytic graphite (HOPG) support by means of a joint experimental and theoretical study.

[a] *Department of Chemistry, Johns Hopkins University, Baltimore, Maryland 21218, USA. E-mail: kbowen@jhu.edu*
[b] *Department of Physics, University of Konstanz, 78464 Konstanz, Germany*
[c] *Department of Materials Science, University of Maryland, College Park, Maryland 20742, USA. E-mail: mkukla@nsf.gov*
[d] *Department of Physics, Tulane University, New Orleans, Louisiana 70118, USA*

† Electronic supplementary information (ESI) available. See DOI: 10.1039/c7cp08427g

Dimethyl methylphosphonate belongs to the large class of organophosphate compounds well known for their toxicity[16,17] but due to its low vapor pressure, its lower toxicity than other compounds in its class, and its structural similarity, it is commonly used as a simulant compound of more hazardous nerve agents such as sarin and soman. $(MoO_3)_3$ trimer clusters have already become the object of many experimental and theoretical studies due to their activity and selectivity in activation of some alkane molecules and dehydration of alcohols.[18–20]

In this work, X-ray photoelectron spectroscopy (XPS) and temperature programmed reaction (TPR) were used to investigate the fate of DMMP on $(MoO_3)_3$ clusters. Density function theory (DFT)-based calculations were used to simulate the adsorption configurations and the decomposition pathways of the DMMP molecule on $(MoO_3)_3$ clusters. The XPS and TPR results showed desorption of intact DMMP and decomposition of DMMP on $(MoO_3)_3$ clusters under elevated temperatures with methanol found to be the major gas-phase product. The theoretical investigation suggested a ''reverse Mars–van Krevelen mechanism'' where reduced oxide clusters and hydroxylated oxide clusters were the active species leading to the decomposition of DMMP associated with the elimination of methanol.

2 Methods

2.1 Experimental method

Molybdenum oxide trimer clusters $(MoO_3)_3$ were prepared as negative cluster anions by a magnetron sputtering source. The magnetron setup consisted of a molybdenum target placed in a magnetic field and biased to -500 V while a mixture of argon, helium and oxygen gases was introduced. The argon gas was ionized to create argon cations, which sputtered the metal target to produce molybdenum atoms and electrons. After reacting with the oxygen to form oxides, the resulting metal oxides aggregated, attached electrons, and formed molybdenum oxide cluster anions. The added helium served to cool and transport the cluster anions down the beamline, where they were then electrostatically accelerated before entering a magnetic sector mass spectrometer (25° sector magnet with resolution of $m/\Delta m = 20$). By tuning the magnetic field strength, $(MoO_3)_3^-$ cluster anions were mass-selected and focused by ion optics before entering the deposition chamber, where they were soft-landed (<1 eV) onto a freshly peeled HOPG substrate (1 cm $\times$ 1 cm) in an ultra-high vacuum (UHV) environment (1×10^{-9} Torr). The graphite-based substrate was specifically chosen to mimic the carbon support traditionally used for MoO_3 based catalysts. The resulting sample can be cooled to approximately -160 °C by liquid nitrogen (LN_2) or heated *via* resistive heating by passing current through the HOPG, with the temperature of the sample being monitored by a K-type thermocouple spring-loaded to the back of the HOPG.

Once clusters had been deposited onto the HOPG substrate, a TPR set-up, using a Hiden HAL/3F PIC quadrupole mass spectrometer (QMS), was used to characterize their activity. The reaction products that desorbed from the surface during a linear temperature ramp were detected and identified by a QMS which was positioned normal to the plane of the substrate and at a distance of 5 mm. To minimize the contribution from background gases and maximize the sensitivity towards species desorbing directly from the substrate, the QMS ionizer was surrounded by a custom-built glass shroud. Typically, in the TPR experiment, 0.2 Langmuir of DMMP was first dosed onto a freshly peeled HOPG surface cooled to -160 °C. The DMMP was purified by several freeze–pump–thaw cycles before being background dosed through a UHV compatible leak valve. After that, 3.0×10^{12} $(MoO_3)_3$ clusters were deposited into the multilayers of DMMP formed on the cooled HOPG. By depositing $(MoO_3)_3$ clusters into DMMP layers, the clusters will preferentially interact with the surrounding DMMP molecules rather than sintering. The number of clusters deposited was calculated by integrating the ion current over the deposition time. During the TPR temperature ramp, the surface temperature was first raised to 0 °C to desorb the vast majority of physisorbed DMMP, and eventually to 450 °C with a ramping rate of 2 °C s^{-1}.

In addition, the deposited samples could also be transferred *in situ* to an adjacent UHV analytic chamber, where they were characterized by X-ray Photoelectron Spectroscopy (*in situ* XPS) with non-monochromatic Mg Kα-rays (1253.6 eV), with the ejected electron kinetic energy analyzed *via* a high energy hemispherical analyzer. In the XPS analytic chamber, the sample was *in situ* heated by e-beam heating with the temperature measured by a K-type thermocouple connected to the sample holder. For the XPS studies, a higher pressure of DMMP (5×10^{-7} Torr) was dosed during the cluster deposition in order to saturate the adsorption sites on $(MoO_3)_3$ before being transferred to XPS analytic chamber. In this case the deposition was performed with the substrate at room temperature to minimize the adsorption of DMMP onto the sample holder.

2.2 Density functional theory calculations

Calculations were performed with DFT[21,22] using a series of modern hybrid functions including, the B3LYP functional,[23,24] its long-range corrected version CAM-B3LYP,[25] and a B3LYP+D3 functional including Grimme's empirical dispersion.[26] In addition to the three variations of the B3LYP functional, a recently developed meta-generalized-gradient (meta-GGA) functional SCAN[27,28] was also employed for calculations of desoprtion energies. The double-ζ 6-31+G(d,p) basis set was used for the H, C, O, and P atoms. The LanL2DZ basis set,[29–31] including the Los Alamos effective core potential, was used for the Mo atoms. Vibrational frequencies were calculated for relevant atomic configurations to distinguish energy minima and transition states. The stationary points corresponding to the energy minima were positively identified by having no imaginary frequencies, and the transition states were confirmed to have exactly one imaginary frequency. Reaction paths were investigated by conducting intrinsic reaction coordinate computations using the Hessian-based predictor–corrector integrator algorithm[32,33] for each transition state. All calculations were carried out with the Gaussian09 code.[34] The modified version

of the Gausian 03 code[35] was used to perform calculations with the SCAN functional.

Coordinates of structures corresponding to DMMP adsorption on stoichiometric $(MoO_3)_3$ and non-stoichiometric Mo_3O_8 and $Mo_3O_9H_n$ (n = 1–3) clusters as well as transition states and products of studied decomposition reactions are collected in ESI.†

3 Results

3.1 XPS characterization of DMMP on $(MoO_3)_3$ Clusters

The temperature dependent XPS spectra of the P(2p) region for DMMP on $(MoO_3)_3$/HOPG are displayed in Fig. 1. As shown in the Fig. 1(a), the P(2p) peak of DMMP on $(MoO_3)_3$ at room temperature was centered at 133.5 eV, compared to the 134.0 eV in the control case of DMMP adsorbed on clean HOPG. The slightly lower binding energy of the P(2p) peak indicates that the phosphorus present in DMMP was partially reduced at room temperature after the DMMP bound to the $(MoO_3)_3$ cluster. After heating the sample to 200 °C and allowing it to cool back to room temperature, the binding energy of the P(2p) peak shifted slightly to an even lower binding energy of 133.1 eV (Fig. 1(b)). Further annealing to higher temperatures (300 °C and 400 °C) shifted the P(2p) peak back to the original position (Fig. 1(c and d)), possibly due to the formation of a PO_x species, which was previously seen with DMMP on other oxides.[7]

The temperature dependent XPS spectra of the Mo(3d) region for $(MoO_3)_3$/HOPG with DMMP adsorption is shown in Fig. 2. The XPS spectra for the Mo(3d) of $(MoO_3)_3$ at room temperature displayed a doublet peak, $3d_{5/2}$ and $3d_{3/2}$, centered at 232.5 eV and 235.6 eV, respectively (Fig. 2(a)). The binding

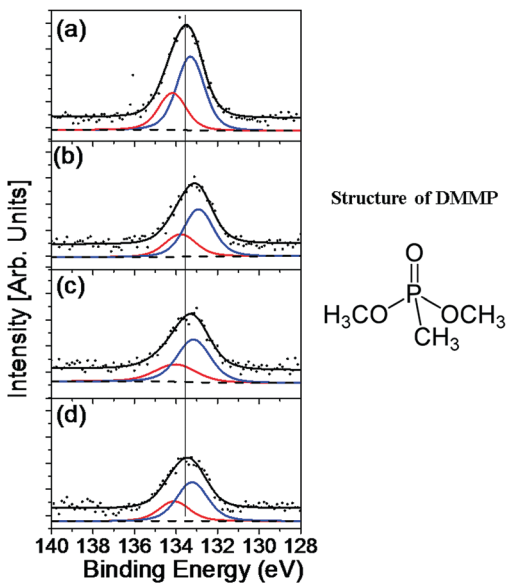

Fig. 1 XPS spectra of the P(2p) envelope of DMMP adsorbed on $(MoO_3)_3$ clusters on HOPG as a function of annealing temperature (a) room temperature (b) 200 °C (c) 300 °C (d) 400 °C. The structure of DMMP is shown on the right.

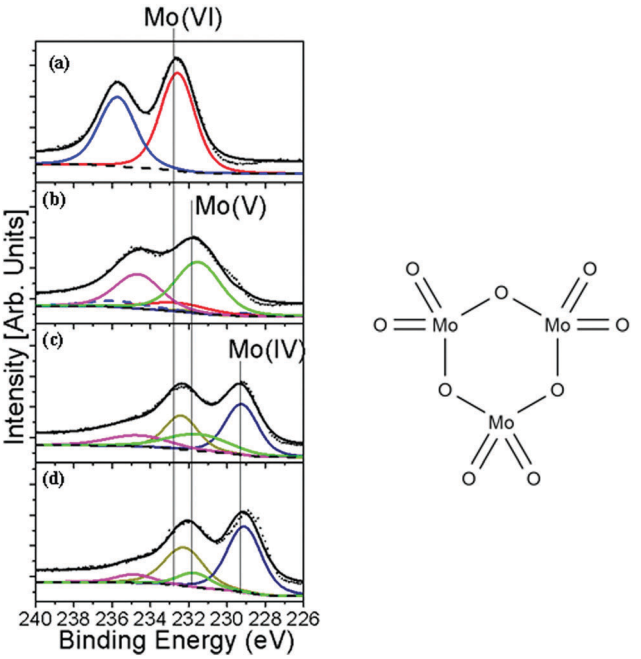

Fig. 2 XPS spectra of the Mo(3d) envelope of $(MoO_3)_3$ clusters on HOPG as a function of annealing temperature (a) room temperature (b) 200 °C (c) 300 °C (d) 400 °C. The structure of the $(MoO_3)_3$ cluster is shown on the right.

energy of $Mo(3d_{5/2})$ is consistent with the binding energy of $Mo(3d_{5/2})$ in Mo(VI), indicating the presence of MoO_3.[36] After heating to 200 °C (Fig. 2(b)), the binding energy of Mo(3d) shifted to a lower binding energy, which indicates that MoO_3 was reduced. Further annealing to 300 °C and 400 °C caused more reduction, resulting in a mixture of lower oxidation species, *i.e.* Mo(IV) and Mo(V). (Fig. 2(c and d)) It has to be noted that the reduction of MoO_3 was also observed in the absence of DMMP adsorption on a HOPG surface, indicating an abundance of reduced Mo species under elevated temperature.

Since the size of the clusters deposited on HOPG are smaller than the inelastic mean free path of photoelectrons generated in XPS, the XPS data can be used to quantize the speciation and concentration of the DMMP on $(MoO_3)_3$ clusters. The relative atomic ratio of P to Mo at different temperatures was calculated and is shown in Fig. 3. This ratio was calculated by dividing the peak area of P(2p) and Mo(3d) with their respective relative sensitivity factor (RSF) and comparing the resulting values. The as-deposited DMMP on $(MoO_3)_3$ ratio of P to Mo is around 0.32. This indicates that for every $(MoO_3)_3$ cluster, about one DMMP molecule ($\sim$0.96) is adsorbed to it. It's worth noting that the ratio of P to Mo decreased with increasing temperature from room temperature to 200 °C. The loss of phosphorus upon heating is possibly due to the desorption of intact DMMP and other phosphorus-containing products. The decrease in the P to Mo ratio is dramatic from room temperature to 200 °C, and flat from 200 °C to 400 °C, indicating the majority of DMMP and other phosphorous containing species desorbed during the temperature range of room temperature to 200 °C.

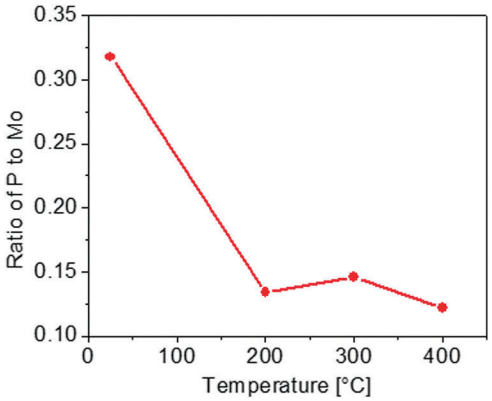

Fig. 3 The relative atomic ratio of P to Mo of DMMP on $(MoO_3)_3$ clusters as a function of annealing temperature.

3.2 Temperature programmed reaction of DMMP on $(MoO_3)_3$

The TPR profiles of DMMP on $(MoO_3)_3$ clusters are recorded in Fig. 4, for the masses of 124 amu, 79 amu, 46 amu, 32 amu, 31 amu, 16 amu, 15 amu, and 2 amu. The mass of 124 amu corresponds to the parent ion of DMMP, while the mass of 79 amu is ascribed to the major fragment of DMMP under electron impact ionization in the QMS. The mass of 46 amu corresponds to dimethyl ether, while 32 and 31 amu are the masses for methanol and its deprotonated form, methoxy, respectively. Masses 16, 15, and 2 amu are methane, methyl, and hydrogen respectively. The TPR profiles of DMMP on HOPG without clusters are included in the ESI† (Fig. S1).

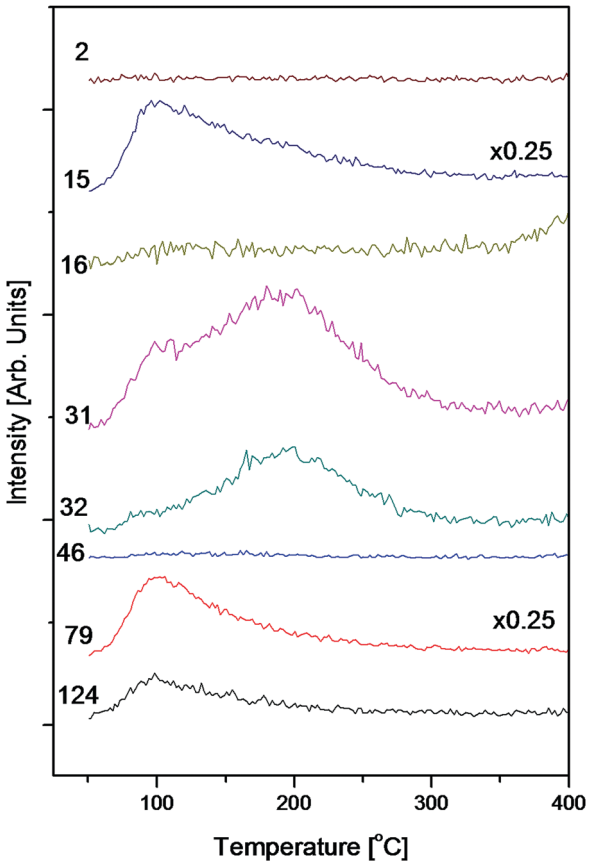

Fig. 4 Temperature programmed reaction profile of DMMP on $(MoO_3)_3$. Each trace corresponds to a mass in amu indicated by the number on the left. Details of each mass are discussed in the body of the paper.

Both 124 and 79 amu showed the same desorption profiles, with a desorption peak centered at 100 °C. This is consistent with the XPS result showing that the majority of DMMP desorbed in the temperature range of RT to 200 °C. Using the Redhead Analysis[37] a desorption energy of 23.4 kcal mol^{-1} was determined for DMMP. For the masses of 32 and 31 amu, a broad desorption peak was observed in both cases, indicating the production of methanol upon heating. The peak position, centered around 200 °C, gives a desorption energy of 29.8 kcal mol^{-1} for methanol. The lower temperature shoulder at 107 °C in the 31 amu profile is a minor fragment from DMMP. No peaks were observed resulting from H_2 (2 amu), CH_4 (16 amu), and dimethyl ether (46 amu). The desorption profile of 15 amu replicated the desorption profile of DMMP and is a minor fragment of DMMP. Subtraction of the DMMP contribution reveals an additional shoulder around 198 °C, corresponding to a desorption energy of 29.7 kcal mol^{-1} for the methyl group (see Fig. S2, ESI†). It is worth mentioning that the TPR experiment has been repeated multiple times for $(MoO_3)_3$ clusters and similar peak shape and positions were observed during these experiments.

3.3 DFT modeling of DMMP adsorption on molybdenum oxide clusters

Oxygen vacancies and hydroxyl groups are common defects on metal oxide surfaces. In previous studies of DMMP on stoichiometric MoO_3 and on defect-rich MoO_3 surface, it was found that the oxygen defects and surface hydroxyls are critical to drive the adsorption and decomposition process of DMMP on the reduced metal oxide surface. At the same time, the stoichiometric oxide surface shows little or no activity and is characterized by a low binding strength to DMMP due to the lack of Lewis acid sites.[13,14] As indicated in XPS measurements (Fig. 2(b–d)) $(MoO_3)_3$ can be easily reduced to nonstoichiometric molybdenum oxide on the graphite support upon exposure to elevated temperatures. In addition, the reduced Mo center can readily promote the dissociation of water at vapor pressure below 10^{-8} Torr,[38] leading to the formation of hydroxylated molybdenum oxide clusters.[13,14] Therefore, in the simulations of adsorption and decomposition of DMMP on molybdenum oxide clusters, several models were considered (Fig. 5 and 6). The models include a DMMP molecule adsorbed on: (1) a stoichiometric cluster, $(MoO_3)_3$ (Fig. 5(b)), (2) a reduced cluster, Mo_3O_8 (Fig. 5(c)), and (3) a series of hydroxylated clusters $Mo_3O_9H_n$ (n = 1–3, Fig. 6(a–h)).

Adsorption of DMMP on $(MoO_3)_3$. Calculations show that the most stable configuration of DMMP adsorbed on the $(MoO_3)_3$ cluster corresponds to the structure in which the DMMP molecule is oriented with its phosphoryl oxygen inside the cluster ring with the methyl and methoxy groups placed between the oxygen atoms of the cluster (Fig. 5(b)). This is consistent with previous studies on Al_2O_3, MgO and WO_3,[6]

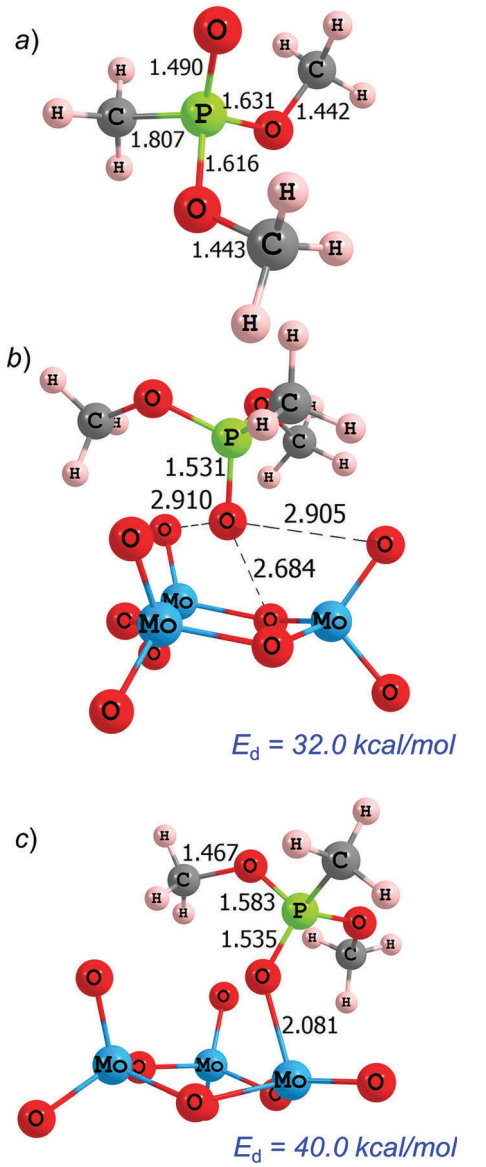

Fig. 5 The structures of the (a) isolated DMMP molecule, (b) molecule adsorbed on a $(MoO_3)_3$ cluster, and (c) molecule adsorbed on a reduced Mo_3O_8 cluster. Desorption energies (shown in blue) were calculated using B3LYP+D3 functional and included ZPVE corrections.

where the phosphoryl oxygen binds to Lewis acid sites, *i.e.* the metal ion center. The resulting structures indicate that there is no additional adsorption sites available on the $(MoO_3)_3$ clusters for adsorbing another DMMP molecule, leaving one DMMP adsorbed on one $(MoO_3)_3$. This is consistent with XPS measurements (see Fig. 3) and additionally explains the estimated ratio of P to Mo (that is $\sim$0.32).

Fig. 5(b) shows a noticeable elongation of the P–O bond (by $\sim$0.04 Å) and shortening of the P–OCH_3 bond (by $\sim$0.02–0.04 Å) in DMMP adsorbed on $(MoO_3)_3$ clusters, as compared with the gas-phase molecule. The distances of the P–CH_3 and O–CH_3 bonds change slightly (by $\sim$0.01 Å) when DMMP is adsorbed on $(MoO_3)_3$.

The desorption energy of DMMP on $(MoO_3)_3$, calculated using B3LYP, is 17.7 kcal mol^{-1} (Table 1). The desorption energy obtained using the long range corrected CAM-B3LYP functional (24.1 kcal mol^{-1}) is $\sim$6 kcal mol^{-1} higher than B3LYP estimation, whereas the inclusion of van der Waals interactions *via* Grimme's empirical dispersion tends to increase the resulting desorption energy by additional $\sim$8 kcal mol^{-1} (32.0 kcal mol^{-1}). A similar trend is observed for the different adsorption configurations of DMMP on the stoichiometric and reduced clusters (Table 1). The desorption energies, recalculated using the meta-GGA SCAN functional, developed for an accurate prediction of weak nonbonding interactions,[28] are consistent with B3LYP+D3 estimations. We therefore will refer in our discussion of the desorption energies to the numbers obtained with the B3LYP+D3 functional.

Adsorption of DMMP on Mo_3O_8 and $Mo_3O_9H_n$ (n = 1–3). The DMMP adsorption on the reduced Mo_3O_8 cluster was simulated (Fig. 5(c)). The DMMP adsorbed molecule has a slightly shortened P–OCH_3 (by $\sim$0.015 Å) and elongated PO–CH_3 (by $\sim$0.015 Å) bonds as compared to the DMMP molecule adsorbed on an ideal $(MoO_3)_3$ cluster (Fig. 5(b)). The calculated desorption energy is 40.0 kcal mol^{-1} (Fig. 5(c) and Table 1), which is 8.0 kcal mol^{-1} higher than that on pristine $(MoO_3)_3$. The trend is consistent with previous studies on MoO_3 thin films, where oxygen defects were found to strengthen the binding of DMMP to molybdenum oxides.[13,14]

There is a negligible change in bond distances of the DMMP molecule adsorbed on the hydroxylated cluster in comparison to DMMP adsorbed on an ideal cluster (Fig. 5(b) and 6(a)). The desorption energy of the DMMP molecule from the hydroxylated cluster is calculated to be 28.6 kcal mol^{-1} (Fig. 6(a) and Table 1). The desorption energies obtained for different configurations of DMMP on $Mo_3O_9H_2$ and $Mo_3O_9H_3$ clusters fall in the range 19–28 kcal mol^{-1} (Fig. 6(b–h) and Table 1). Regardless of the number of hydrogens on the clusters, the binding of DMMP to hydroxylated clusters happens to be comparable or even weaker than the binding to the stoichiometric $(MoO_3)_3$ clusters. This observation differs from the previous studies on MoO_3 thin films, where the hydroxylated MoO_3 surface was found to provide much stronger adsorption, as compared to the pristine MoO_3 surface.[13,14] It was suggested that the pristine MoO_3 surface binds weakly to DMMP due to the lack of Lewis acid sites at the terminal oxygen layer.[13,14] Given the substantial structural difference between the pristine MoO_3 surface and the $(MoO_3)_3$ clusters, a different binding energy with DMMP should be expected for $(MoO_3)_3$ clusters. A direct comparison of the calculated desorption energies from MoO_3 surface and $(MoO_3)_3$ clusters is problematic because different computational schemes were used. Nonetheless, it's plausible that the strong Lewis acidity and also the open six-member ring structure of $(MoO_3)_3$ accommodate the DMMP molecule better than the pristine oxide surface both sterically and energetically.

3.4 DFT modeling of DMMP decomposition on molybdenum oxide clusters

The decomposition mechanisms of an isolated DMMP molecule and adsorbed on a molybdenum oxide clusters were studied using the CAM-B3LYP functional. Although the

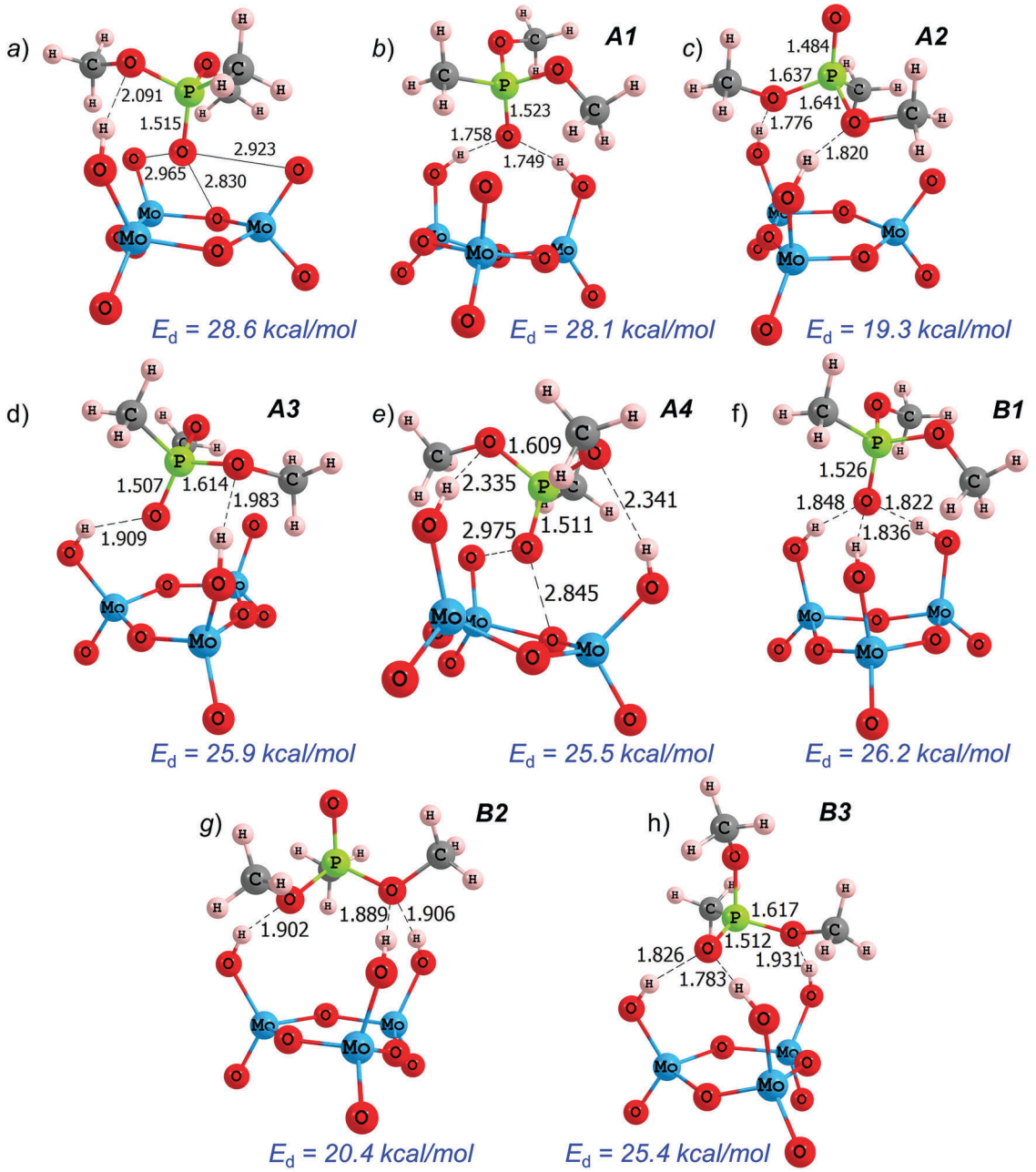

Fig. 6 The structures of the DMMP molecule adsorbed on the hydroxylated clusters in several configurations are shown: (a) Mo_3O_9H, (b–e) $Mo_3O_9H_2$, and (f–h) $Mo_3O_9H_3$ clusters. Desorption energies (shown in blue) were calculated using B3LYP+D3 functional and included ZPVE corrections.

CAM-B3LYP functional underestimates energies of the DMMP desorption from $(MoO_3)_3$ relative to the B3LYP+D3 method, the decomposition energies obtained using these functionals were found to be in good agreement (Table S1 of ESI†).

To simulate the decomposition of DMMP, we analyzed the six most feasible reactions. They include: (1) the cleavage of the P═O (eqn (1), Path 1, Fig. 7), (2) P–CH_3 (eqn (2), Path 2, Fig. 7), (3) O–CH_3 (eqn (3), Path 3, Fig. 7), and (4) P–OCH_3 (eqn (4), Path 4, Fig. 7) bonds, (5) the concerted intramolecular elimination of methanol (eqn (5), Path 5, Fig. 7), and (6) the methanol elimination involving the intermolecular (cluster-to-molecule) hydrogen transfer that can occur on the hydroxylated $Mo_3O_9H_n$ (n = 1, 2) clusters (eqn (6), Path 6, Fig. 7). The obtained activation barriers and reaction energies are collected in Table 2.

$$(CH_3)PO(OCH_3)_2 \rightarrow (CH_3)P(OCH_3)_2 + {}^3O_{(atom)} \quad (1)$$

$$(CH_3)PO(OCH_3)_2 \rightarrow {}^\bullet PO(OCH_3)_2 + {}^\bullet CH_3 \quad (2)$$

$$(CH_3)PO(OCH_3)_2 \rightarrow (CH_3)PO(OCH_3)O^\bullet + {}^\bullet CH_3 \quad (3)$$

$$(CH_3)PO(OCH_3)_2 \rightarrow (CH_3)P^\bullet O(OCH_3) + {}^\bullet OCH_3 \quad (4)$$

$$(CH_3)PO(OCH_3)_2 \rightarrow (CH_2)PO(OCH_3) + HOCH_3 \quad (5)$$

Table 1 Calculated and experimental desorption energies (in kcal mol^{-1}) of the DMMP molecule from the molybdenum oxide clusters

Cluster/configuration		Theory							
		B3LYP		CAM-B3LYP		B3LYP+D3		SCAN[a]	
		E	E+ZPVE	E	E+ZPVE	E	E+ZPVE	E	Exp.
Mo_3O_9		19.1	17.7	25.6	24.1	33.8	32.0	35.7	23.4
Mo_3O_8		29.5	28.6	35.4	34.2	41.4	40.0	35.8	
Mo_3O_9H		15.5	13.8	21.9	19.9	30.7	28.6	31.4	
$Mo_3O_9H_2$	***A1***	19.1	17.1	22.9	20.6	30.1	28.1	25.6	
	A2	9.6	7.8	12.3	10.2	21.3	19.3	15.7	
	A3	15.9	14.0	20.3	18.2	28.0	25.9	23.5	
	A4	—		20.0	17.9	27.2	25.5	26.9	
$Mo_3O_9H_3$	***B1***	19.2	17.4	27.4	25.4	28.3	26.2	23.8	
	B2	11.2	9.6	19.8	18.0	22.6	20.4	15.0	
	B3	19.5	17.6	20.7	18.5	27.6	25.4	21.9	

[a] Total energies were refined through a single point calculation using the geometry structure optimized with B3LYP+D3 functional.

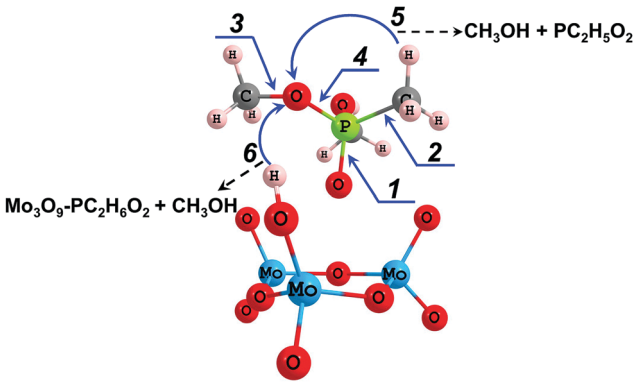

Fig. 7 Schematic representation of decomposition channels of DMMP: fission of (1) P═O (eqn (1)), (2) P–CH_3 (eqn (2)), (3) O–CH_3 (eqn (3)), (4) P–OCH_3 (eqn (4)) bonds, (5) the methanol elimination through a concerted intramolecular hydrogen transfer (eqn (5)), and (6) the methanol elimination through the intermolecular hydrogen transfer.

$$H_n(MoO_3)_3\text{-}(CH_3)PO(OCH_3)_2 \rightarrow H_{n-1}(MoO_3)_3\text{-}(CH_3)PO(OCH_3) + HOCH_3 \quad (6)$$

In the isolated DMMP molecule, the P═O bond breaking requires the highest energy (130.7 kcal mol^{-1}) among all probed reactions. The P–OCH_3 bond cleavage is a noticeably less costly process (93.1 kcal mol^{-1}), whereas the P–CH_3 and O–CH_3 bond breaking requires ~10 kcal mol^{-1} less energy (84.0 and 83.3 kcal mol^{-1}, respectively). The elimination of methanol is the most energetically favorable process with an activation barrier of 67.5 kcal mol^{-1}. These findings are consistent with results of the recent study reporting methyl and methanol, among other products, of DMMP pyrolysis in the gas-phase.[39]

Once DMMP is adsorbed on ideal $(MoO_3)_3$ clusters, its decomposition requires even higher energy than decomposition of the isolated DMMP molecule (Table 2). For example, the

Table 2 Calculated and experimental activation barriers (in kcal mol^{-1}) of DMMP decomposition in the gas phase and adsorbed on molybdenum oxide clusters

Reaction	DMMP	DMMP adsorbed on Mo oxide cluster				
		Mo_3O_9	Mo_3O_8	Mo_3O_9H	$Mo_3O_9H_2$	Exp
1 P═O	130.7	—	—	—	—	—
2 P–CH_3	84.0	90.5	56.4	75.8	75.5	—
3 O–CH_3	83.3	91.3	22.1	30.7	20.6	29.7
4 P–OCH_3	93.1	95.9	68.1	87.6	70.3	—
5 CH_3OH loss (intramolecular)	67.5	72.3	70.7	71.5	71.4	29.8
6 CH_3OH loss (intermolecular)	—	—	—	23.9	20.0	

energy required for the cleavage of P–CH_3 and O–CH_3 bonds increases by ~6–8 kcal mol^{-1}. The methanol elimination remains the most favorable process and requires ~20 kcal mol^{-1} lower energy (72.3 kcal mol^{-1}) than the homolysis of the P–CH_3 (90.5 kcal mol^{-1}), O–CH_3 (91.3 kcal mol^{-1}) and P–OCH_3 (95.9 kcal mol^{-1}) bonds. Thus, the ideal stoichiometric $(MoO_3)_3$ clusters would serve to stabilize the adsorbed DMMP molecule rather than degrading it.

Reduced Mo_3O_8 clusters behave notably differently. Significantly lower energies are characteristic for the decomposition of DMMP on the reduced Mo_3O_8 clusters as compared to the isolated molecule and ideal clusters (Table 2). For instance, the O–CH_3 bond cleavage needs only 22.1 kcal mol^{-1} instead of 91.3 kcal mol^{-1} on the ideal $(MoO_3)_3$ cluster, showing a dramatic drop in activation energy. Table 2 shows a ~30 kcal mol^{-1} decrease of the P–CH_3 and P–OCH_3 bond energies relative to similar reactions of the DMMP molecule on an ideal cluster. Unlike these, the methanol loss reaction is barely affected by the lack of oxygen atom in the cluster configuration. The activation barrier predicted for methanol elimination from the DMMP molecule on Mo_3O_8 cluster (70.7 kcal mol^{-1}) is only 1.6 kcal mol^{-1} lower than in the molecule adsorbed on the ideal $(MoO_3)_3$ cluster (72.3 kcal mol^{-1}) and 3.2 kcal mol^{-1} higher than in gas-phase (67.5 kcal mol^{-1}). Interestingly, the O–CH_3 bond cleavage is the dominating reaction (rather than the methanol elimination) on the Mo_3O_8 clusters.

The decomposition of the DMMP molecule adsorbed on a hydroxylated Mo_3O_9H cluster *via* bond cleavage pathways requires lower energies than the gas-phase DMMP or DMMP on the ideal cluster (Table 2). The energies of the P–OCH_3 (87.6 kcal mol^{-1}), P–CH_3 (75.8 kcal mol^{-1}), and O–CH_3 (30.7 kcal mol^{-1}) bonds cleavage are 8.3, 14.7, and 60.6 kcal mol^{-1} lower relative to the DMMP molecule adsorbed on an ideal cluster. The methanol elimination *via* intramolecular hydrogen transfer (eqn (5), Path 5, Fig. 7) requires 71.5 kcal mol^{-1} and is only 0.8 kcal mol^{-1} lower than the activation barrier calculated for DMMP on the ideal cluster (72.3 kcal mol^{-1}).

Hydroxylated clusters bring about an opportunity for intermolecular hydrogen transfer activated reactions. Thus, the methanol loss from DMMP on hydroxylated clusters may also proceed *via* intermolecular hydrogen transfer (eqn (6), Path 6, Fig. 7) unlike the similar reaction proceeding through intramolecular

hydrogen transfer in the isolated molecule, on the ideal or reduced clusters. Table 2 shows that this reaction channel dominates DMMP decomposition in the presence of hydroxyl groups and requires the activation energy as low as 23.9 kcal mol^{-1} on the hydroxylated Mo_3O_9H clusters and 20.0 kcal mol^{-1} on the $Mo_3O_9H_2$ clusters.

For the O–CH_3 bond dissociation, the reaction competing with the methanol loss, in the DMMP molecule adsorbed on the $Mo_3O_9H_2$ cluster (20.6 kcal mol^{-1}) needs 10 kcal mol^{-1} lower energy than that on a Mo_3O_9H cluster (30.7 kcal mol^{-1}), whereas the activation barrier of intermolecular methanol elimination (eqn (6), Path 6, Fig. 7) is 20 kcal mol^{-1}. The intramolecular elimination of methanol remains high energy reaction that requires 71.4 kcal mol^{-1} and can be triggered at high temperature.

We conclude here that methanol loss reactions are dominating decomposition mechanisms in the isolated DMMP and DMMP on ideal stoichiometric clusters; the reactions are activated with a fairly high energy of $\sim$70 kcal mol^{-1}, implying that DMMP is rather stable in these configurations and does not decompose well. The reduced clusters favor the O–CH_3 fission decomposition pathway with the low activation barrier of $\sim$22.1 kcal mol^{-1} and barely affect the methanol elimination barrier. The hydroxylated clusters catalyze two competing channels, the O–CH_3 fission and the methanol loss through intermolecular hydrogen transfer with low activation energies of 20–30 kcal mol^{-1} while the intramolecular hydrogen transfer reaction would be still viable at high temperature ($\sim$70 kcal mol^{-1}).

4 Discussion

4.1 Adsorption and desorption of DMMP on $(MoO_3)_3$

Our results allow us to analyze the adsorption characteristics of DMMP on $(MoO_3)_3$. The XPS results indicate that the initial adsorption of DMMP onto $(MoO_3)_3$ can occur at room temperature. The XPS spectra of the P(2p) region of DMMP on $(MoO_3)_3$ at room temperature already contained partially reduced phosphorus as shown in Fig. 1(a), although our theory shows that stoichiometric $(MoO_3)_3$ clusters do not decompose DMMP well. In addition, previous studies in UHV suggested little or no decomposition of DMMP on stoichiometric MoO_3 at low pressure.[14] We speculated that the presence of partially reduced phosphorus at room temperature could be caused by some nonstoichiometric Mo_3O_{9-x} cluster species present on HOPG, which have the capability to decompose DMMP, similar to the reduced MoO_3 surface.[13] It is interesting to note that each $(MoO_3)_3$ cluster adsorbs about one DMMP molecule evident from a 1 : 3 P to Mo ratio from XPS envelope fitting, possibly due to steric effects and limited adsorption sites on the clusters. This is in good agreement with the results of our theoretical modeling, which show that the binding energy of a second DMMP molecule (12.5 kcal mol^{-1}) is $\sim$8 kcal mol^{-1} lower than that of the first (19.5 kcal mol^{-1}). In addition, the P to Mo ratio observed here is significantly higher than that observed in MoO_3 thin films,[13] probably due to the high dispersion of these isolated $(MoO_3)_3$ clusters as well as their higher binding affinity to DMMP resulting from their increased Lewis acidity as compared to bulk MoO_3.[20]

Additionally, the decreasing of the P to Mo ratio in XPS upon heating (Fig. 3) and the TPR results (Fig. 4) provide some insight into the desorption behavior of DMMP on these clusters. The TPR profile of both the DMMP parent ion (124 amu) and its major fragment (79 amu) exhibited a desorption peak around 100 °C, which is consistent with the large decrease in the P to Mo ratio from RT to 200 °C. This resulted in a desorption energy, as calculated *via* Redhead Analysis, of about 23.4 kcal mol^{-1} (Table 1). Upon comparing to theory, the desorption energy of DMMP from $(MoO_3)_3$ clusters falls in the range of theoretically calculated values for DMMP desorbed from stoichiometric $(MoO_3)_3$ clusters (32 kcal mol^{-1}), Mo_3O_9H clusters (28.6 kcal mol^{-1}), $Mo_3O_9H_2$ clusters (19.3–28.1 kcal mol^{-1}), and $Mo_3O_9H_3$ clusters (20.4–26.2 kcal mol^{-1}), (Fig. 5, 6 and Table 1). The experimentally determined desorption energy is calculated from the peak center of the DMMP desorption profiles (124 and 79 amu), but when the broadness and skewness of the peaks are considered it indicates the presence of a range of desorption energies (Fig. 4). Given the little information known about the nature and energetics of adsorption sites, a direct spectral deconvolution will be premature here. However, the broad range of desorption energies can be explained by a non-homogenous composition in the deposited clusters. Such non-homogenous composition for the deposited clusters will consequently affect the decomposition of DMMP as discussed below.

4.2 Decomposition of DMMP on molybdenum oxide clusters

What are the reaction pathways and the reaction products of DMMP on $(MoO_3)_3$ and its reduced forms?

First, the reduction of the phosphorus of DMMP on $(MoO_3)_3$ was seen in XPS at elevated temperatures, indicated by a shift of P(2p) peak to lower binding energy (Fig. 1(b)). Previous studies on titania and ceria assigned the reduced phosphorus species to methyl methylphosphonate and methyl phosphonate due to a stepwise loss of methoxy groups.[7,40] The TPR results in this work showed the evolution of methanol indicating that methoxy groups pick up a hydrogen and evolve into the gas phase leaving behind methyl methylphosphonate, which is similar to the case of DMMP on titania and ceria.[7] This also agrees well with previous ambient pressure XPS studies on defect-rich MoO_3 surface, which suggested a loss of methanol during DMMP decomposition.[13] However, the desorption energy of methanol from Redhead Analysis of TPR (29.8 kcal mol^{-1}) is significantly lower than the calculated activation barrier of methanol elimination from the DMMP molecule adsorbed on the stoichiometric $(MoO_3)_3$ (72.3 kcal mol^{-1}) and the non-stoichiometric Mo_3O_8 (70.7 kcal mol^{-1}) clusters (Table 2). This discrepancy between the experimental value and theoretical prediction is still substantial even after taking the underestimation of the frequency factor used in Redhead analysis into account. Alternatively, according to the results of our theoretical modeling, the presence of hydroxyls on the cluster may cause an approximately four-fold reduction of the energy required for methanol elimination (Table 2 and Fig. 8). The calculated activation barrier for methanol

loss *via* cluster-to-molecule hydrogen transfer (eqn (6), Fig. 7 and 8) requires 20–24 kcal mol^{-1} which are comparable to the experimentally estimated activation energy of 29.8 kcal mol^{-1} (Table 2).

The proposed intermolecular hydrogen transfer mechanism is in agreement with earlier results on metal oxide surfaces indicating the important role of surface hydroxyls as nucleophiles in methanol elimination from DMMP.[6] Recent XPS studies from Head *et al.* also suggested the presence of neighboring surface hydroxyls is responsible for the methanol elimination.[13] We note, although the initial clusters deposited onto the graphite surface are stoichiometric $(MoO_3)_3$, the elevated surface temperature can easily lead to the formation of the reduced metal center, which promotes the dissociation process of residual water molecules to form hydroxylated metal oxide even at UHV conditions. It is evident from our study that the importance of surface defects and hydroxyl groups is also applicable to the corresponding cluster species.

An analysis of the decomposition energies, collected in Table 2, revealed that the loss of a methyl group from DMMP seen in the TPR (Fig. 4) with an activation energy of 29.7 kcal mol^{-1} can be explained by the O–CH_3 bond cleavage in the DMMP molecule adsorbed on a reduced Mo_3O_8 and hydroxylated $Mo_3O_9H_n$ (n = 1, 2) clusters. Our calculations determined the decomposition energy of this bond cleavage are 22.1 (Mo_3O_8), 30.7 (Mo_3O_9H) and 20.6 ($Mo_3O_9H_2$) kcal mol^{-1} (Table 2 and Fig. 8), in good agreement with experiment. This indicates some level of structure sensitivity in the decomposition of DMMP between the different stoichiometries of clusters with the non-stoichiometric Mo_3O_8 cluster preferentially removing a methoxyl methyl group and the Mo_3O_9H cluster preferentially removing an intact methoxy group *via* methanol elimination, while the $Mo_3O_9H_2$ cluster supports DMMP decomposition along either pathway.

The results of our joint experimental and theoretical study revealed the effect of surface hydroxyl and reducible metal centers on the reaction pathway and product distributions of DMMP decomposition. The activation energies required for methanol and methyl loss from DMMP adsorbed on $Mo_3O_9H_n$ (n = 1, 2) and Mo_3O_8 clusters are 3–4 times lower compared to the gas-phase and decomposition on the ideal stoichiometric cluster. Practically, reduced Mo_3O_8 can be easily generated by thermal reductions of Mo_3O_9 clusters on graphite support and hydroxylated clusters are immediate products of residual water and reduced metal oxide clusters. A full catalytic cycle can be viewed as a water-assisted "reverse Mars–van Krevelen mechanism".[41,42] The bond cleavage of DMMP is driven by reduced metal oxides (Mo^{4+} and Mo^{5+}) and the presence of water facilitates the formation of the methanol *via* an intermolecular hydrogen transfer mechanism. The reduced metal oxides can be easily regenerated under thermal treatment due to a high reducibility of Mo metal center within the clusters on graphite support.[43] It is interesting to note that in previous studies regeneration of metal oxides is usually carried out by thermal annealing under oxygen environment.[41,44] This procedure usually resulted in a higher affinity to DMMP but a lower activity toward decomposition.[44] The higher affinity to DMMP is likely due to an increase in Lewis acidity from the presence of PO_x.[45] According to the mechanism we proposed here, oxygen annealing would not recover the oxygen vacancies thus a low activity toward DMMP decomposition was found. To further

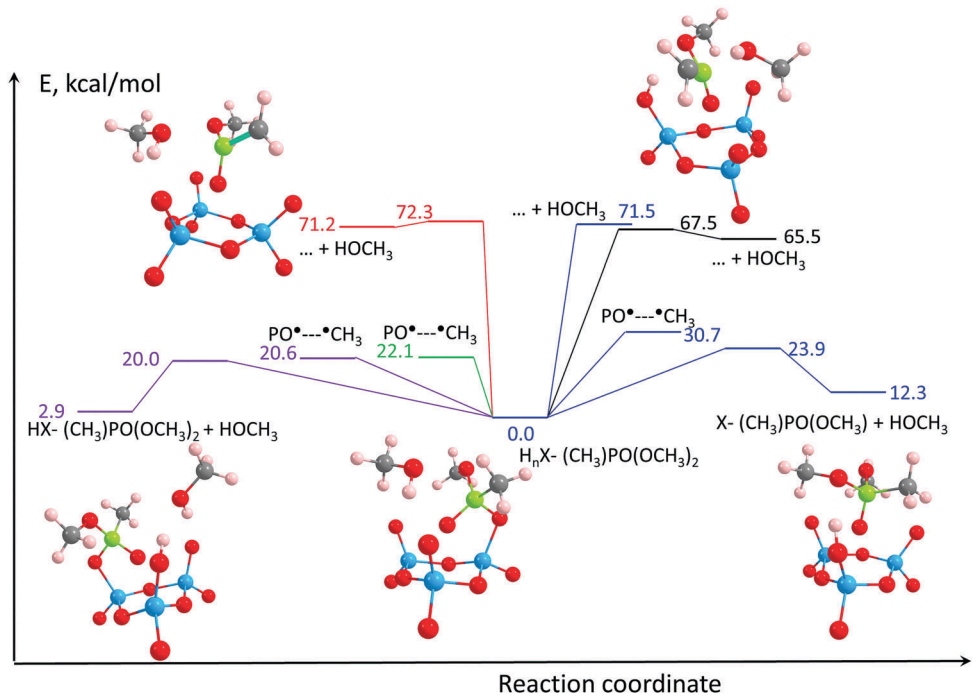

Fig. 8 Schematic energy diagram for the decomposition of DMMP. Blue lines correspond to decomposition pathways of DMMP adsorbed on a Mo_3O_9H cluster, purple – $Mo_3O_9H_2$, green – Mo_3O_8 cluster, red – $(MoO_3)_3$ cluster, and black – gas phase.

verify the proposed mechanism, two different metal oxide clusters, *i.e.* $(WO_3)_3$ and $(ZrO_2)_3$ were chosen to study the relationship between the reducibility of metal center and their reactivity toward DMMP. The study is currently ongoing. Last, a possible inference with the proposed catalytic route is the potential poison effect of the residual PO_x species left on the MoO_3 surface. However, this may not be practically significant given the relatively cheap cost of MoO_3 oxides and also the low concentrations of the phosphorus species.

5 Conclusion

The adsorption and decomposition behaviors of DMMP on size-selected $(MoO_3)_3$ clusters were studied experimentally by XPS and TPR and theoretically by DFT calculations. The experimental results indicated that the decomposition of DMMP on $(MoO_3)_3$ involves the loss of methoxy groups leading to the elimination of methanol during the reaction, and the experiments provided the measured desorption energies that helped validate the theoretical calculations. The theoretical calculations determined that hydroxyl groups on the cluster and partially reduced, non-stoichiometric, clusters had significantly lowered activation barriers for DMMP decomposition, showing the importance of the reducibility of a metal center and the presence of residual hydroxyl groups in metal oxide catalysis. The Group VI transition metal oxide based cluster materials are potential candidates for adsorption and decomposition of CWA with similar structures to DMMP due to their structural fluxionality and Lewis acidity. A combination of XPS and TPR measurements coupled with DFT modeling is a powerful methodology to explore how chemical activity and selectivity of the clusters towards decomposition of CWA compounds depends on their structure and chemical composition. This knowledge could be further used for rational design of new materials with targeted catalytic properties.

Conflicts of interest

There are no conflicts to declare.

Acknowledgements

This material is based upon work supported by the Defense Threat Reduction Agency (DTRA) under grant number HDTRA1-15-1-0005. R. T. and M. M. K acknowledge support from DOE NERSC resources (Contract DE-AC02-05CH11231). MMK is grateful to the Office of the Director of National Science Foundation for support under the IRD program.

References

1 S. Yenisoy-Karakas, A. Aygun, M. Gunes and E. Tahtasakal, *Carbon*, 2004, **42**, 477–484.
2 B. Aurianblajeni and M. M. Boucher, *Langmuir*, 1989, **5**, 170–174.
3 C. N. Rusu and J. T. Yates, *J. Phys. Chem. B*, 2000, **104**, 12292–12298.
4 L. Yang, D. Tunega, L. Xu, N. Govind, R. Sun, R. Taylor, H. Lischka, W. A. DeJong and W. L. Hase, *J. Phys. Chem. C*, 2013, **117**, 17613–17622.
5 V. M. Bermudez, Quantum-Chemical Study of the Adsorption of DMMP and Sarin on γ-Al_2O_3, *J. Phys. Chem. C*, 2007, **111**, 3719–3728.
6 M. B. Mitchell, V. N. Sheinker and E. A. Mintz, *J. Phys. Chem. B*, 1997, **101**, 11192–11203.
7 D. A. Chen, J. S. Ratliff, X. F. Hu, W. O. Gordon, S. D. Senanayake and D. R. Mullins, *Surf. Sci.*, 2010, **604**, 574–587.
8 A. R. Wilmsmeyer, J. Uzarski, P. J. Barrie and J. R. Morris, *Langmuir*, 2012, **28**, 10962–10967.
9 A. R. Wilmsmeyer, W. O. Gordon, E. D. Davis, D. Troya, B. A. Mantooth, T. A. Lalain and J. R. Morris, *J. Phys. Chem. C*, 2013, **117**, 15685–15697.
10 D. E. Taylor, K. Runge, M. G. Cory, D. S. Burns, J. L. Vasey, J. D. Hearn, K. Griffith and M. V. Henley, *J. Phys. Chem. C*, 2013, **117**, 2699–2708.
11 D. Troya, A. C. Edwards and J. R. Morris, *J. Phys. Chem. C*, 2013, **117**, 14625–14634.
12 Y. Paukku, A. Michalkova and J. Leszczynski, *J. Phys. Chem. C*, 2009, **113**, 1474–1485.
13 A. R. Head, R. Tsyshevsky, L. Trotochaud, Y. Yu, L. Kyhl, O. Karslioglu, M. M. Kuklja and H. Bluhm, *J. Phys. Chem. C*, 2016, **120**, 29077–29088.
14 A. R. Head, *et al.*, *Catal., Struct. React.*, 2017, **3**, 112–118.
15 L. Trotochaud, R. Tsyshevsky, S. Holdren, K. Fears, A. R. Head, Y. Yu, O. Karslıoğlu, S. Pletincx, B. Eichhorn, J. Owrutsky, J. Long, M. Zachariah, M. M. Kuklja and H. Bluhm, *Chem. Mater.*, 2017, **29**, 7483–7496.
16 Y. C. Yang, J. A. Baker and J. R. Ward, *Chem. Rev.*, 1992, **92**, 1729–1743.
17 K. Kim, O. G. Tsay, D. A. Atwood and D. G. Churchill, *Chem. Rev.*, 2011, **111**, 5345–5403.
18 G. Fu, X. Xu, X. Lu and H. Wan, *J. Am. Chem. Soc.*, 2005, **127**, 3989–3996.
19 G. Fu, X. Xu, X. Lu and H. Wan, *J. Phys. Chem. B*, 2005, **109**, 6416–6421.
20 X. Tang, D. Bumueller, A. Lim, J. Schneider, U. Heiz, G. Ganteför, D. H. Fairbrother and K. H. Bowen, *J. Phys. Chem. C*, 2014, **118**, 29278–29286.
21 P. Hohenberg and W. Kohn, *Phys. Rev. B: Condens. Matter Mater. Phys.*, 1964, **136**, B864.
22 W. Kohn and L. J. Sham, *Phys. Rev.*, 1965, **140**, 1133.
23 C. T. Lee, W. T. Yang and R. G. Parr, *Phys. Rev. B: Condens. Matter Mater. Phys.*, 1988, **37**, 785–789.
24 A. D. Becke, *J. Chem. Phys.*, 1993, **98**, 5648–5652.
25 T. Yanai, D. P. Tew and N. C. Handy, *Chem. Phys. Lett.*, 2004, **393**, 51–57.
26 S. Grimme, J. Antony, S. Ehrlich and H. Krieg, *J. Chem. Phys.*, 2010, **132**, 154104.
27 J. W. Sun, A. Ruzsinszky and J. P. Perdew, *Phys. Rev. Lett.*, 2015, **115**, 036402.

28 J. Sun, *et al.*, *Nat. Chem.*, 2016, **8**, 831–836.
29 P. J. Hay and W. R. Wadt, *J. Chem. Phys.*, 1985, **82**, 270–283.
30 P. J. Hay and W. R. Wadt, *J. Chem. Phys.*, 1985, **82**, 299–310.
31 W. R. Wadt and P. J. Hay, *J. Chem. Phys.*, 1985, **82**, 284–298.
32 H. P. Hratchian and H. B. Schlegel, *J. Chem. Phys.*, 2004, **120**, 9918–9924.
33 H. P. Hratchian and H. B. Schlegel, *J. Chem. Theory Comput.*, 2005, **1**, 61–69.
34 M. J. Frisch, *et al.*, *Gaussian 09*, Gaussian, Inc., Wallingford, CT, USA, 2009.
35 M. J. Frisch, *et al.*, *Gaussian 03, Revision D.02*, Gaussian, Inc., Wallingford CT, USA, 2004.
36 X. Li, K. A. Wepasnick, X. Tang, Y. Wang, K. H. Bowen, D. H. Fairbrother and G. Gantefoer, *J. Vac. Sci. Technol., B*, 2012, **30**, 031806.
37 J. L. Falconer and J. A. Schwarz, *Catal. Rev.: Sci. Eng.*, 1983, **25**, 141–227.
38 H. Bluhm, *J. Electron Spectrosc. Relat. Phenom.*, 2010, **177**, 71–84.
39 S. Y. Liang, P. Hemberger, N. M. Neisius, A. Bodi, H. Grutzmacher, J. Levalois-Grutzmacher and S. Gaan, *Chem. – Eur. J.*, 2015, **21**, 1073–1080.
40 J. Zhou, K. Varazo, J. E. Reddic, M. L. Myrick and D. A. Chen, *Anal. Chim. Acta*, 2003, **496**, 289–300.
41 T. M. Tesfai, V. N. Sheinker and M. B. Mitchell, *J. Phys. Chem. B*, 1998, **102**, 7299–7302.
42 A. V. Mironenko and D. G. Vlachos, *J. Am. Chem. Soc.*, 2016, **138**, 8104–8113.
43 Z. J. Li, Z. T. Fang, M. S. Kelley, B. D. Kay, R. Rousseau, Z. Dohnalek and D. A. Dixon, *J. Phys. Chem. C*, 2014, **118**, 4869–4877.
44 D. A. Panayotov and J. R. Morris, *Langmuir*, 2009, **25**, 3652–3658.
45 M. Ai and S. Suzuki, *J. Catal.*, 1973, **30**, 362–371.

